Surface & Coatings Technology 496 (2025) 131684

Contents lists available at ScienceDirect

Surface & Coatings Technology

journal homepage: www.elsevier.com/locate/surfcoat

Functionalized graphite nanosheet/organosilicon composite coatings with soft-hard structures: Excellent wear resistance and hydrogen barrier properties

Chilou Zhou [a,*], Yanlei Huang [a], Xianhui Liu [a], Yan Huang [b], Hao Wu [b,c,**], Zhengli Hua [d], Paul K. Chu [c], Yansheng Yin [b]

[a] School of Mechanical and Automotive Engineering, South China University of Technology, Guangzhou 510641, China
[b] Guangdong Key Laboratory of Materials and Equipment in Harsh Marine Environment, School of Naval Architecture and Ocean Engineering, Guangzhou Maritime University, Guangzhou 510725, China
[c] Department of Physics, Department of Materials Science and Engineering and Department of Biomedical Engineering, City University of Hong Kong, Tat Chee Avenue, Kowloon, Hong Kong, China
[d] Institute of Process Equipment, Zhejiang University, Hangzhou 310027, China

ARTICLE INFO

Keywords:
Rubber seals
Modified graphite nanosheet
Hydrogen seals
Wear resistance
Hydrogen barrier
Hydrogen permeation

ABSTRACT

Rubber seals for hydrogen energy equipment face reciprocating wear and hydrogen permeation, which can lead to seal failure. Constructing protective coatings with both wear resistance and hydrogen barrier functions on rubber surfaces is an encouraging solution. In this study, a unique "soft-hard" structure is proposed and demonstrated. In this structure, the soft modified graphite (MG) nanosheets are incorporated into the hard-organosilicon sol, and then MG nanosheets/organosilicon composite coatings are deposited on nitrile butadiene rubber (NBR) substrates surface by the spin-coating technique. The composite coatings exhibit excellent wear resistance and hydrogen barrier properties, and the coatings with an appropriate concentration have strong adhesion to the substrate. The friction coefficient and hydrogen permeability coefficient of NBR-MG6 are 0.11 and 2.12×10^{-9} ($mol \cdot m^{-1} \cdot s^{-1} \cdot MPa^{-1}$) with the modified graphite of 6 mg/ml, respectively. Compared with the pure NBR, the friction coefficient and hydrogen permeability coefficient of NBR-MG6 decrease by 90.8 % and 51 %, respectively. The introduction of MG nanosheet enhances the adhesion between the coating and the substrate, which forms a self-lubricating film during the wear process, thereby enhancing the wear resistance of the sample. Furthermore, MG nanosheets form a barrier layer within the coating, extending the diffusion path of hydrogen molecules and adsorbing nearby hydrogen, thereby reducing the permeability. This work reveals new strategies for the design of protective coatings for rubber seals in hydrogen energy equipment.

1. Introduction

Nowadays, the world is facing increasingly severe challenges such as energy shortages, climate change, and environmental pollution [1,2]. In this context, hydrogen energy has garnered significant attention as an emerging energy vector due to its extensive availability of resources, high energy conversion efficiency, and zero pollution advantages [3–5]. Hydrogen storage and transportation are crucial aspects of the hydrogen energy industry. Polymer materials are widely used in hydrogen storage and transportation equipment, including plastic liners (high density polyethylene (HDPE), polyamide (PA) and polyethylene terephthalate (PET)) for hydrogen storage cylinders and rubber seals (ethylene propylene diene monomer (EPDM), nitrile butadiene rubber (NBR) and fluororubber (FKM)) and polytetrafluoroethylene (PTFE) gaskets for sealing components. Due to the extremely small hydrogen molecules, polymer materials used in high-pressure hydrogen equipment are required to have low hydrogen permeability. Hydrogen permeability coefficients of different polymer materials at specific hydrogen pressures and temperatures are summarized in Table 1:

Among these polymer materials, rubber sealing materials exhibit

* Corresponding author.
** Correspondence to: H. Wu, Guangdong Key Laboratory of Materials and Equipment in Harsh Marine Environment, School of Naval Architecture and Ocean Engineering, Guangzhou Maritime University, Guangzhou 510725, China.
E-mail addresses: mezcl@scut.edu.cn (C. Zhou), haowu.academic@gmail.com (H. Wu).

https://doi.org/10.1016/j.surfcoat.2024.131684
Received 6 June 2024; Received in revised form 24 November 2024; Accepted 16 December 2024
Available online 17 December 2024

Table 1
Hydrogen permeability coefficients of different polymer materials.

Materials	Pressure (MPa)	Temperature (°C)	Hydrogen permeability coefficients ($\times10^{-10}$ mol·m^{-1}·s^{-1}·MPa^{-1})
HPDE [6]	10	30	9.25
PA [7]	0.1	25	3.68
PET [8]	0.1	25	11.1
EPDM [9]	0.1	25	170
NBR [9]	0.1	25	38
FKM [9]	0.1	25	21
PTFE [10]	0.35	26	13.27

high hydrogen permeability, which can adversely affect high-pressure hydrogen sealing. In the sealing structures, hydrogen leakage arises from three factors: (1) hydrogen permeation through sealing elements, (2) leakage caused by mechanical damage to sealing elements, and (3) leakage through gaps between sealing elements and devices, among which permeation leakage and mechanical damage leakage are extremely difficult to avoid [11]. More importantly, the accumulation of hydrogen molecules in rubber can lead to performance degradation, such as hydrogen-induced blister fracture [12,13] and hydrogen-induced swelling [14,15], posing significant safety hazards to high-pressure hydrogen sealing. Wear constitutes the typical mechanical damage of rubber seals in high-pressure hydrogen gas dynamic sealing applications [16,17]. The high friction of rubber is mainly attributed to its viscoelastic nature, rendering it vulnerable to adhering to the mating surface and producing lagging wear. Furthermore, adhesive and abrasive wear aggravate the wear tendency of rubber. In the high-pressure environment, hydrogen is prone to leaking from the wear position of rubber, leading to seal failure.

Currently, the construction of coatings on material surfaces is considered an effective strategy for protection. Wear-resistant coatings on material surfaces have been extensively researched [18–21]. Nakahigashi et al. [22] have deposited diamond-like carbon coatings onto NBR surfaces using radio-frequency plasma-enhanced chemical vapor deposition technology and observed a reduction of approximately 1.5 times in the friction coefficient of NBR surfaces. Zhou et al. [23] have utilized electron beam dispersion technology to prepare PTFE composite coatings doped with copper acetate and polyethylene (PE) on rubber substrates. Owing to the relatively low surface energy of PE-PTFE, the coatings decrease the dynamic friction coefficient of rubber. Bragaglia et al. [24] have employed the sol-gel technique to prepare organically modified SiO_2 coatings on rubber surfaces, and the SiO_2 coatings show a substantial reduction in the friction coefficient, with a maximum reduction of 30 %. However, the aforementioned studies have solely focused on wear resistance, which may not fulfill the diverse requirements of coatings under complex conditions. Furthermore, in order to reduce the hydrogen permeability of polymeric materials in hydrogen energy equipment, hydrogen barrier coatings have been proposed [8,25–27]. However, the research in this field is not yet mature. Covering the substrate surface with impermeable lamellar materials with a large surface area is an effective way to enhance the hydrogen barrier properties. A polymer-based composite coating comprising hexylamine (HA) functionalized reduced graphene oxide (RGO), and polyurethane has been designed by Bandyopadhyay et al. [28], and the hydrogen gas transmission rate of composite coating PA films with a 43.3 % concentration of RGO-HA decreases by 82 % compared to the pure PA films. The electrostatic layer-by-layer self-assembly technique has been employed to deposit various modified graphene oxide/polyethyleneimine composite films on PET substrates by Zhao et al. [29–31], and these composite films exhibit excellent hydrogen barrier properties. Currently, hydrogen barrier coatings on polymer surfaces are mostly used for hydrogen storage vessel liners, and the tribological properties of such coatings have not yet been reported. At present, only one report on the construction of a dual-functional coating with both wear resistance and gas barrier properties on rubber surface can be found. Cadambi et al. [32] have deposited tungsten carbide coating on the surface of hydrogenated butyl rubber (HNBR) by means of ion implantation process. Permeation and wear tests showed that, compared with the substrate, noticeable reduction in gas transmission rate by 25.6 % and improved resistance to wear by 42.6 % for HNBR coated samples. Owing to the special working environment of rubber seals in high-pressure hydrogen systems and the demanding requirements of coatings, the development of a rubber surface coating with outstanding wear resistance and hydrogen barrier properties is imperative.

To confer dual functionality of wear resistance and hydrogen barrier onto coatings, the materials must possess both self-lubrication and a lamellar structure with a high aspect ratio. Boron nitride [33], layered double hydroxides [34], graphene [30,35], etc. are common two-dimensional layered materials, but their complex preparation process and high cost hinder large-scale industrial applications. As natural lamellar materials, graphite sheets possess potential application value in the gas barrier field due to their abundant production, environmental protection, and low cost [36–39]. More importantly, graphite nanosheets exhibit better tribological properties than thin-layer materials like graphene, which are recognized industrial lubricants [40–43]. When soft graphite nanosheets are combined with hard coatings, they act not only as a lubricating layer, but also as an internal skeleton, to enhance the structural integrity of the coatings.

In this work, graphite nanosheets are modified by the silane coupling agent and then incorporated into the organosilicon sol to prepare modified graphite (MG) nanosheets/organosilicon composite coatings on rubber substrates. The incorporation of MG lubricating nanosheets leads to a significant reduction in the friction coefficient and wear rate. Furthermore, the MG nanosheets act not only as barriers for hydrogen diffusion and extending the diffusion path of hydrogen, but also play a certain adsorption effect on hydrogen [44–46]. Compared to pure NBR, the friction coefficient and hydrogen permeability coefficient of the NBR-MG6 sample decrease by 90.8 % and 51 %, respectively, demonstrating outstanding wear resistance and hydrogen barrier properties. The preparation of composite coatings with both wear resistance and hydrogen barrier functions on rubber by the sol-gel method is innovative. Owing to the environmentally friendliness and low cost of the coatings, the commercial potential of the materials and technique is immense.

2. Experimental details

2.1. Materials

Graphite (5000 mesh, AR), tetraethyl orthosilicate (TEOS, AR), triethoxymethylsilane (MTES, AR), γ-aminopropyltriethoxysilane (KH-550, 99 %), dopamine hydrochloride (DA, 98 %), tris(hydroxymethyl) aminomethane hydrochloride (Tris-HCl, 99 %) and ethanol (AR) were obtained from Shanghai McLean Biochemical Technology Co., Ltd. (China). Hydrochloric acid (HCl, 37 %) was provided by Guangzhou Qianhui Chemical Glass Instrument Co., Ltd. (China). Sodium hydroxide (NaOH, AR) was obtained from Sinopharm Chemical Reagent Co., Ltd. (China). AR indicated that the purity of the reagent was analytical grade. All the reagents were used as received without further purification. NBR samples (thickness of 2 mm for permeability test, and thickness of 4 mm for wear test) purchased from Shenzhen Baoshun Plastic Materials Co., Ltd. (China) were employed as substrates for the tests. Deionized water was produced in our laboratory. The spin coater (KW-4 T) was purchased from the Institute of Microelectronics, Chinese Academy of Sciences (China).

2.2. Pretreatment of NBR substrate

The NBR substrate lacks functional groups, making it challenging for

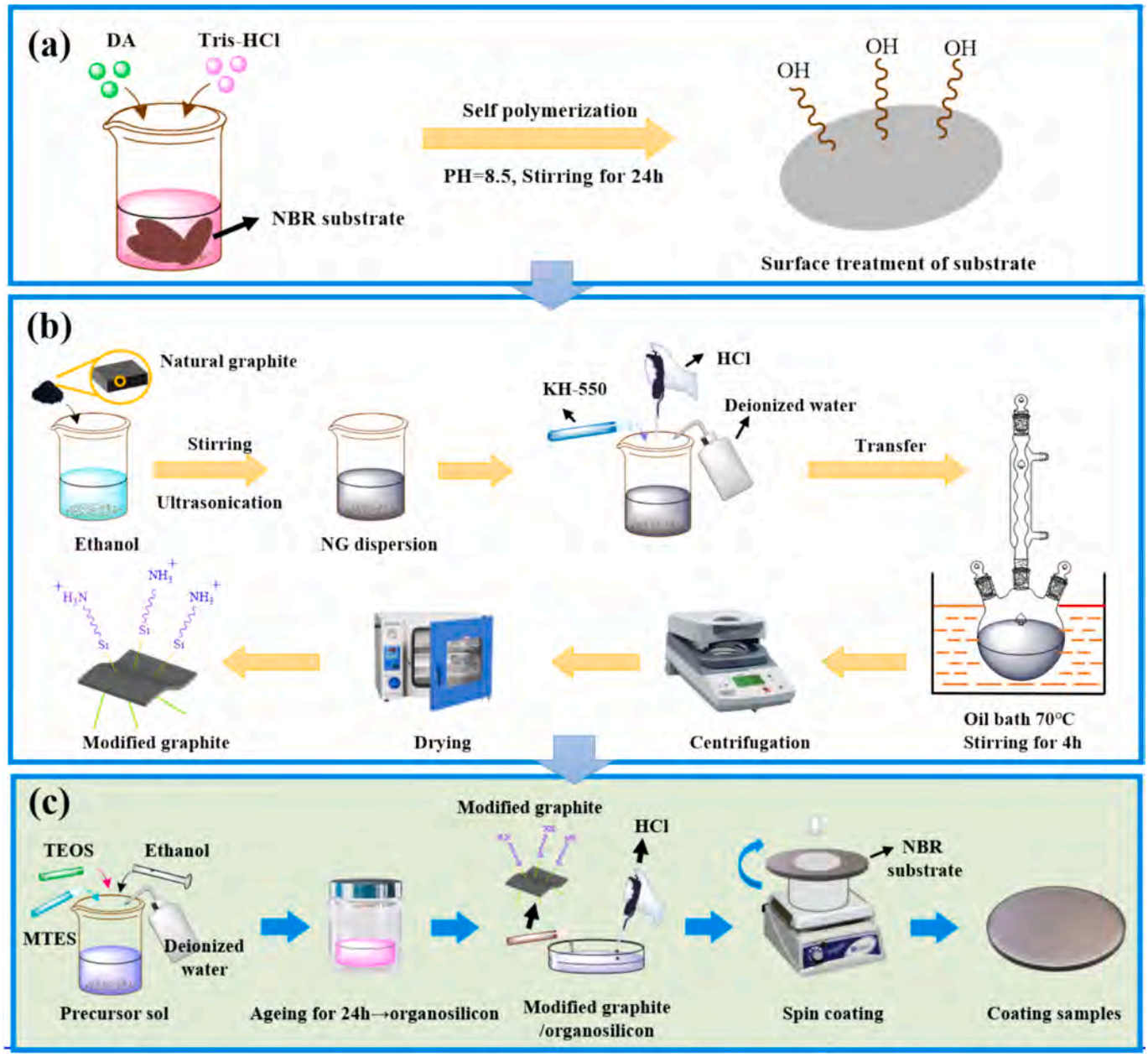

Fig. 1. (a) Pretreatment of the NBR substrate; (b) preparation of modified graphite; (c) schematic showing the preparation of the composite coatings.

its surface to form covalent bonds with coating components. To address this, surface pretreatment of the substrate is necessary. This study utilizes the self-polymerization of dopamine under alkaline conditions, which forms a polydopamine layer on the substrate surface. This process enriches the substrate surface with hydroxyl and amine groups, facilitating the formation of covalent bonds with coating components, thereby enhancing the adhesion of the coating to the substrate.

The NBR samples were first cut into 60 mm diameter pieces and ultrasonically cleaned in ethanol for 10–20 min to remove surface stains. A certain quantity of Tris-HCl was dissolved in deionized water and stirred at room temperature to obtain the 1.2 g/L Tris buffer solution. A certain quantity of dopamine hydrochloride was added to the Tris buffer solution and obtain a 2 g/L dopamine solution after mixing. The pH of the dopamine solution was adjusted by using 1 mol/L NaOH solution to 8.5 to provide an alkaline environment for the self-polymerization of dopamine. Finally, the cleaned rubber substrate was immersed in the configured dopamine solution for the surface polymerization reaction for 24 h, and then washed with deionized water and dried at 60 °C to obtain the pretreated rubber substrate [47]. The schematic diagram of the substrate pretreatment process is presented in Fig. 1(a).

2.3. Modification of graphite

Natural graphite (NG) sheets easily form aggregated stacked structures within organosilicon sol, making it difficult to achieve uniform dispersion within the coating and potentially leading to a decline in coating performance. To fully utilize the excellent barrier and self-lubricating properties of graphite sheets and ensure their uniform distribution in the organosilicon sol, the graphite sheets were modified with KH-550 in this study.

NG (500 mg) was added to 180 ml of ethanol, stirred, and sonication for 30 min to obtain a graphite dispersion. The pre-dispersed graphite was easier to combine with silane coupling agent KH-550. The graphite dispersion, KH-550, deionized water, and hydrochloric acid were mixed with a volume ratio of 9:2.5:1:0.1, transferred to a three-neck flask, heated, and stirred at 70 °C for 4 h using a condensation reflux device.

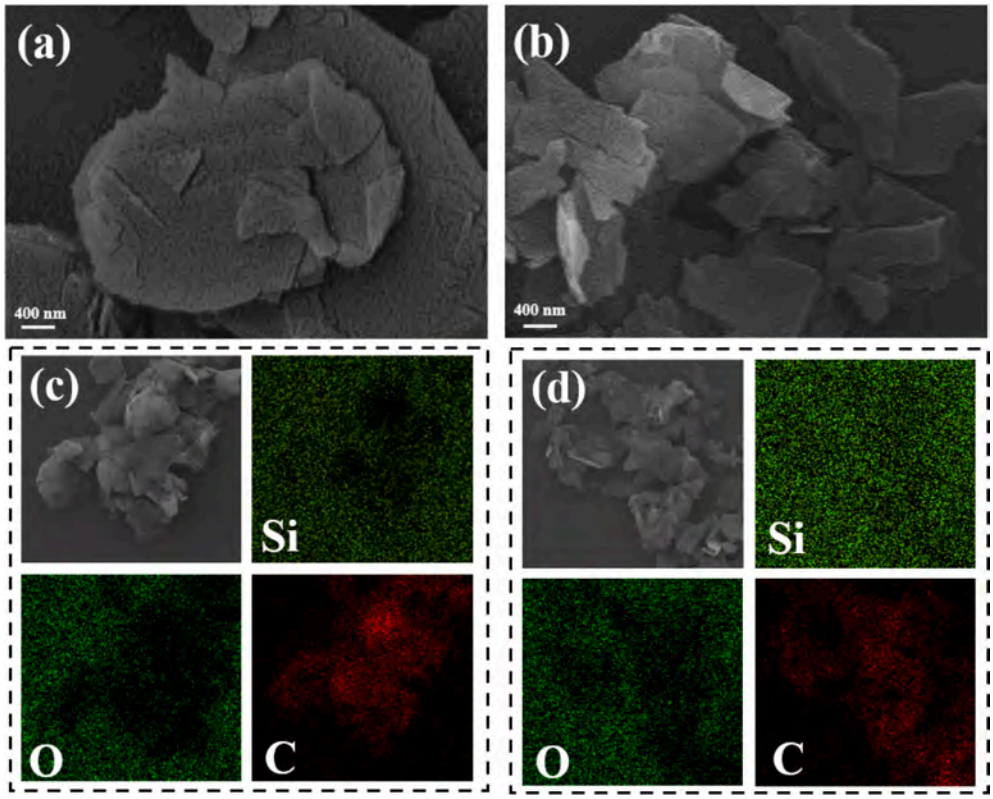

Fig. 2. SEM images of (a) NG nanosheets and (b) MG nanosheets; EDS elemental maps of (c) NG nanosheets and (d) MG nanosheets.

After the reaction, the mixture was washed with ethanol and centrifuged 3–4 times to remove the excess of KH-550 and HCl. The product was vacuum dried at 80 °C for 12 h to obtain the KH-550 modified graphite. The images and corresponding reaction details are shown in Fig. 1(b).

2.4. Preparation of MG/organosilicon composite coating

TEOS, MTES, ethanol, and deionized water were mixed evenly with the ratio of 1:1:2.5:0.5 by volume, stirred continuously for 30 min, sealed, and aged at room temperature for 4 days to obtain the precursor sol. A certain quantity of MG was added to the precursor sol and stirred vigorously to prepare the MG/organosilicon composite sols with concentrations of 0 mg/ml, 2 mg/ml, 4 mg/ml, 6 mg/ml, and 8 mg/ml, respectively. Several drops of HCl were added and stirred for 30 min to promote hydrolysis and cross-linking of precursors (TEOS) and co-precursors (MTES) [48]. The composite sol was transferred to a vacuum dryer until no bubbles emerged from the sol. The pre-treated rubber substrate was fixed on a spin-coating machine, and the composite coatings with different contents of MG were applied dropwise to the substrate. It was spun at a low speed (300–1000 rpm) for 20 s and a high speed (1200–3000 rpm) for 10 s, dried, and cured at 40 °C for 2 h. The coated samples containing different contents of MG were named as NBR-MG0, NBR-MG2, NBR-MG4, NBR-MG6, NBR-MG8. The schematic illustration of the preparation process of composite coatings is presented in Fig. 1(c).

2.5. Characterization

The morphologies and structures of MG and composite coatings were investigated by scanning electron microscopy (SEM, Crossbeam 350, Germany), and the elemental composition and distribution were determined by energy-dispersive X-ray (EDS) spectroscopy. The function groups were determined by Fourier transform infrared (FTIR) spectroscopy (Nicolet IS50, USA) in the range of 500–4000 cm^{-1}. X-ray diffraction (XRD) was carried out on an X-ray polycrystal diffractometer (Rigaku SmartLab SE, Japan) to observe the crystal structures. The zeta potentials of the graphite dispersion before and after KH-550 modification were determined on the nanoparticle analyzer (HORIBA SZ-100Z, Japan). The hydrogen barrier properties of the uncoated substrate and coated samples were determined on the GTR-721 (SYSTESTER, China) gas permeability machine at 1 MPa and 25 °C. Three parallel samples were used for each group of materials to ensure the repeatability of the experiment. GCr15 steel balls (Ø = 6 mm) were employed in ball-on-disk type tribometer tests (UMT TriboLab, Germany). The steel balls acted on the surface of the samples with a load of 2 N and a rate of 200 rad/min, with a friction radius of 5 mm and a test duration of 60 min. After the friction and wear tests, the wear tracks were observed by a white light interferometer (ContourGT-K0, Bruker, Germany).

3. Results and discussion

3.1. Characterization of MG nanosheets

The surface morphology of the NG nanosheets and MG nanosheets are investigated by SEM. Fig. 2(a) and (b) reveals the typical dense laminar structure of the NG nanosheets with predominantly large and dense sheets and some scattered smaller ones. The graphite nanosheets modified by KH-550 display signs of exfoliation, showing a scattered distribution, and some of the sheets exhibit a single-layer structure and the diameter of the graphite sheet is greatly reduced. This phenomenon can be attributed to the hydrolysis of KH-550 in HCl, producing functional groups, such as silanol, that are stably arranged within the interstices of the NG nanosheets. Due to these long organic chains, the graphite sheets are propped up, and the inter-spacing rises significantly. Under constant thermal agitation, the NG nanosheets gradually transform into thin structures, resulting in a reduction in diameter through constant collisions. In order to further verify the modification effect of KH-550, the graphite sheet surface before and after modification is

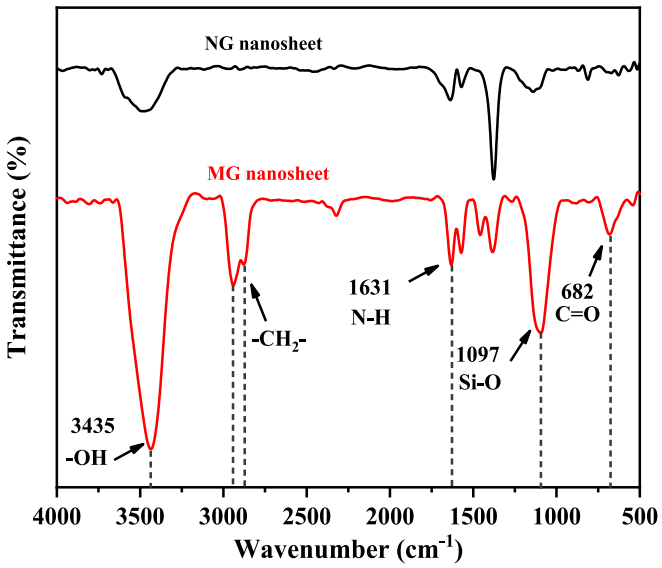

Fig. 3. FTIR spectra of the NG nanosheet and MG nanosheet.

analyzed by EDS, as shown in Fig. 2(c) and (d). For the NG nanosheets, Si and O of the NG nanosheets are obviously missing from the graphite region, while C exhibits high-density distribution characteristics. Conversely, the MG nanosheets have more Si in all the regions. Additionally, O is observed from the graphite region, but the distribution of C is relatively sparse. The results indicate that Si-bearing functional groups, generated by the hydrolysis of KH-550, are grafted onto and uniformly distributed across the surface of the graphite sheets.

The graphite nanosheets before and after modification are analyzed by FTIR. Fig. 3 shows that both natural and modified graphite nanosheets have a stretching band at 3435 cm^{-1} attributed to the presence of -OH groups [49,50]. The MG nanosheets exhibit increased -OH exposure due to interlayer peeling, resulting in heightened intensity of the -OH peak. Compared to the NG nanosheet, the MG nanosheet spectra exhibit weak absorption bands at 2926 cm^{-1} and 2852 cm^{-1} from symmetric and asymmetric -CH_2 stretching, besides peaks at 682 cm^{-1} due to C═O stretching [50]. Strong Si—O stretching bands at 1097 cm^{-1} are observed from the MG nanosheet due to C—N (960 cm^{-1}) and C—C (909 cm^{-1}) bending [49,50]. Moreover, a characteristic peak corresponding to KH-550 (-NH_2 shear vibration) is detected at 1631 cm^{-1}, along with new absorption peaks at 1403 cm^{-1} and 1383 cm^{-1} [49,50]. The results indicate that the hydrolysis product of the silane coupling agent KH-550, silanol (SiOH) groups, which can combine with the oxygen-containing groups of graphite sheets by physical absorption and/or chemical bonds [49]. The above results show that the NG sheet has been successfully modified by KH-550, and the modified graphite sheet can be easily dispersed into the solvent, which has a positive effect on the uniformity and stable distribution of graphite sheet in organosilicon sol.

The zeta potentials are measured to determine the charged state of graphite nanosheets in ethanol before and after modification, as shown in Fig. 4(a). The average potential of the NG nanosheets is 1.1 mV, with a sharp overall potential distribution near 0 mV. This indicates the NG nanosheet is overall electrical neutral and carries almost no charge. In contrast, the average potential of the MG nanosheets increases to 42.4 mV, with a significantly broadening potential distribution curve, indicating that the modification treatment enables the charged functional groups generated by the hydrolysis of KH-550 to combine with the graphite nanosheets, resulting in the positive charge on the graphite nanosheets. The absolute value of the zeta potential indicates the stability of the particle-solution system, with a higher absolute value indicating better dispersion. The KH-550 modification treatment notably enhances the dispersion of the graphite sheet in the ethanol solution. Fig. 4(b) depicts the digital photographs of the graphite nanosheets before and after modification in the organosilicon sol for 0 min, 30 min, 60 min, and 90 min with a content of 5 mg/ml. The NG nanosheets in the organosilicon sol gradually settle, and finally, the nanosheets are completely delaminated with the organosilicon sol. However, the MG nanosheets remain uniformly dispersed in the organosilicon sol throughout the 90 min static test, further confirming the modification effect of KH-550. The above results further corroborate the microscopic morphology and dispersion state of the modified graphite sheets (Fig. 2).

3.2. Characterization of the composite coatings

Fig. 5(a–e) displays the surface micro-morphology of the coatings with different contents of MG nanosheets. All the surfaces exhibit a cracked morphology, attributed to volume contraction and the high stiffness of the sol-gel film during the molding process, which typically induces mechanical stresses during rapid drying, leading to the formation of numerous cracks perpendicular to the surfaces during stress release. The blocky crack morphology is advantageous in preserving the bonding between the hard coating and the substrate and ensuring the protective effect of the coating during significant deformation of the

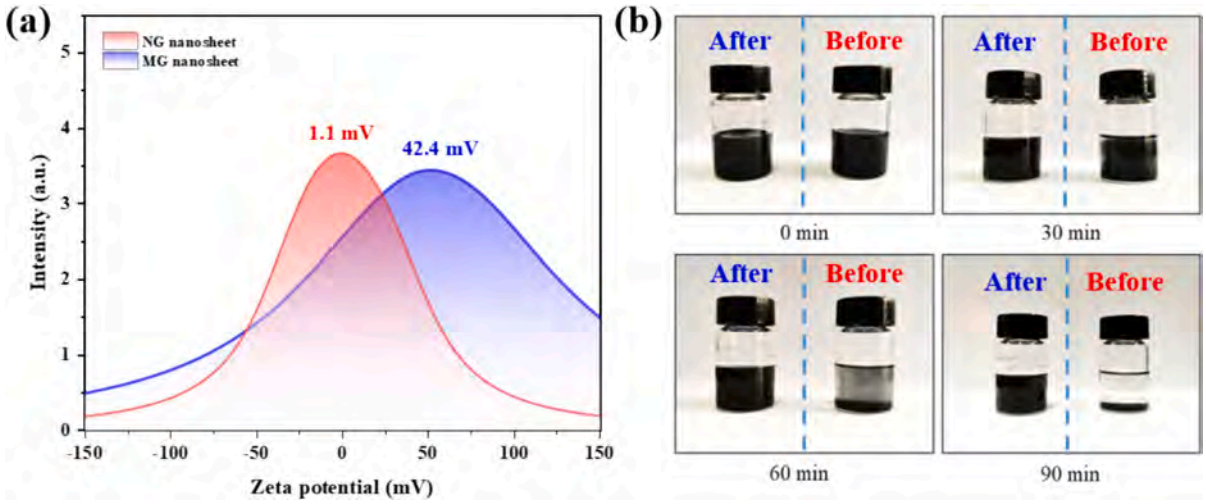

Fig. 4. (a) Zeta potentials of the NG nanosheet and MG nanosheet ethanol dispersion; (b) static tests of the graphite nanosheets before and after modification in the organosilicon sol.

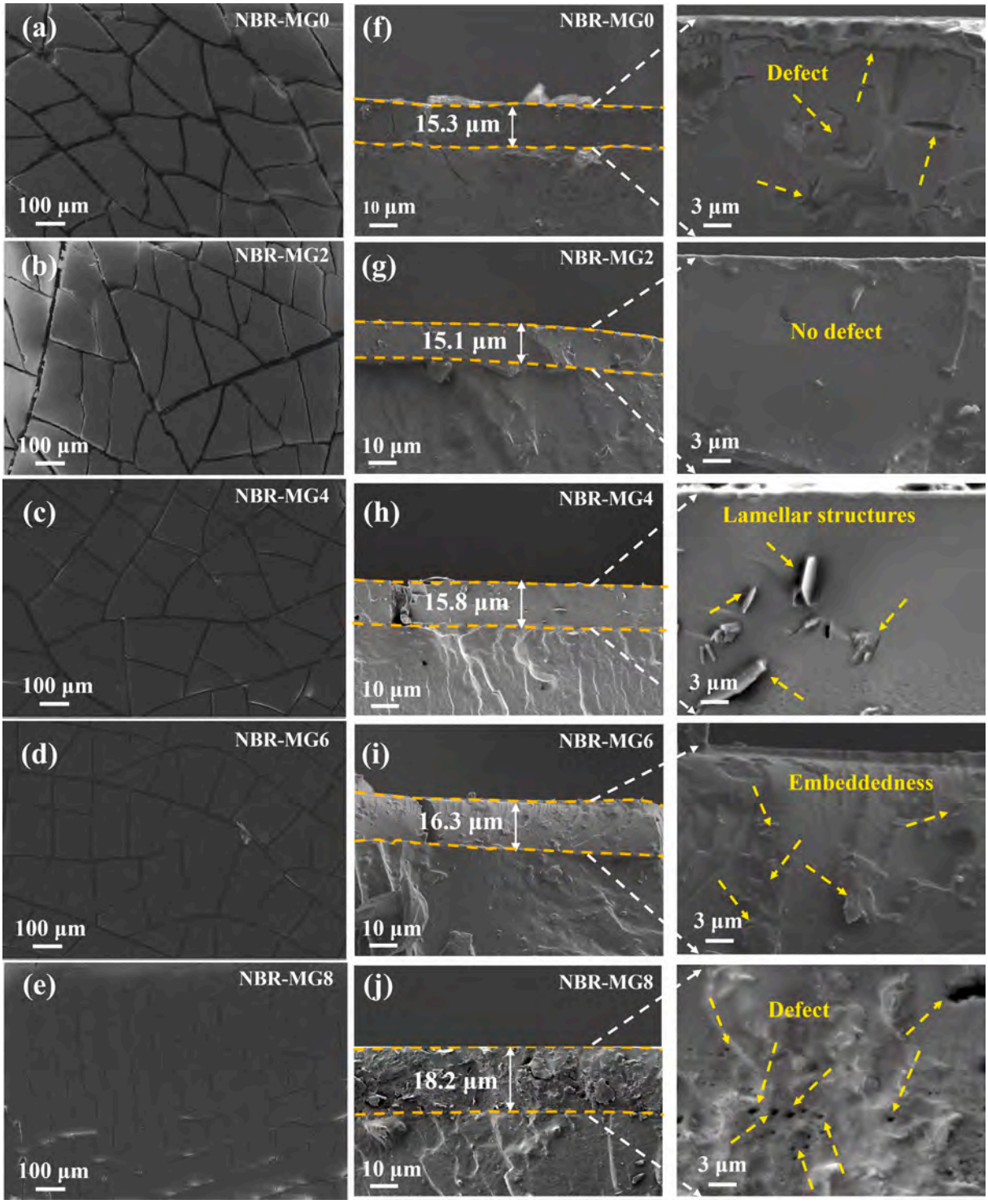

Fig. 5. Surface morphology of (a) NBR-MG0, (b) NBR-MG2, (c) NBR-MG4, (d) NBR-MG6, and (e) NBR-MG8; Cross-sectional morphology of (f) NBR-MG0, (g) NBR-MG2, (h) NBR-MG4, (i) NBR-MG6, and (j) NBR-MG8.

rubber substrate. As shown in Fig. 5(a), a large quantity of debris is observed at the cracks on the surface of NBR-MG0, with minor detachment noticed at certain crack tip locations. This indicates a relatively low overall structural strength of the coating, with large cracks being prone to initiating and propagating internal microcracks, leading to fragmentation at the stress concentration area of the crack tips. When MG nanosheets are introduced, the coating densification of NBR-MG2 is improved, and only a small quantity of debris is observed from the crack interface (Fig. 5(b)). As the content of MG further increases, the surfaces of NBR-MG4 (Fig. 5(c)) and NBR-MG6 (Fig. 5(d)) exhibit a dense state, with the edges of the coating cracks appearing flat and smooth. No additional fine debris is observed at the crack seams together with a noticeable reduction in the spacing between block-like cracks. NBR-MG8 (Fig. 5(e)) shows a significant reduction in crack size, with the average crack size being <100 μm, displaying a rectangular structure with a uniform arrangement and a more compact overall morphology. Fig. 5(f–j) shows the cross-sectional morphology of composite coatings with different contents of MG nanosheets. The coating thicknesses are in

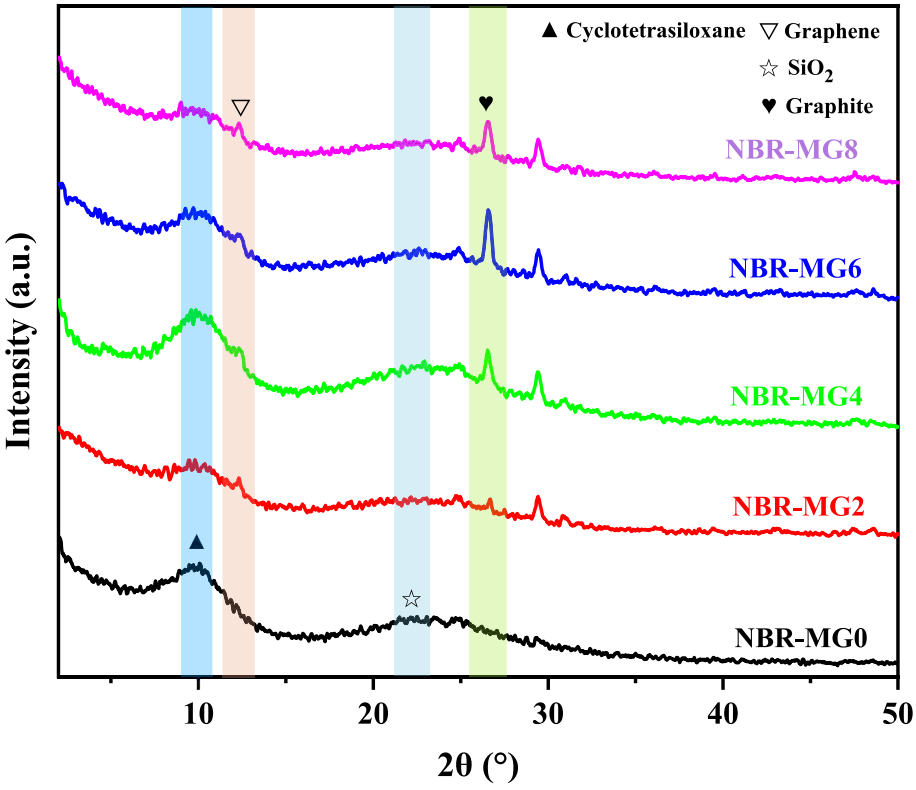

Fig. 6. XRD patterns of NBR-MG0, NBR-MG2, NBR-MG4, NBR-MG6, and NBR-MG8.

the range of 15.1–18.2 μm, among which the thickness of NBR-MG8 is the largest. The coating cross-section of NBR-MG0 (Fig. 5(f)) shows numerous defects, with coating detachment possibly attributed to the numerous internal defects. In contrast, the coating cross-section of NBR-MG2 (Fig. 5(g)) exhibits no significant defects. Furthermore, the coating cross-section of NBR-MG4 (Fig. 5(h)) reveals exposed lamellar structures with a random distribution. In contrast, no distinct lamellar structures are observed from NBR-MG6 (Fig. 5(i)), with the majority embedded in the coating. The cross-sectional roughness of NBR-MG8 (Fig. 5(j)) significantly increases, accompanied by the presence of many pore defects.

The XRD results of the composite coatings with different contents MG sheets are shown in Fig. 6. The characteristic peaks of the pure organosilicon coating are primarily at $2\theta = 9.8°$ and $2\theta = 23°$, corresponding to the peak of cyclotetrasiloxane and amorphous silica, respectively [51,52]. Due to the faster hydrolysis and condensation rates of MTES compared to TEOS, the addition of MTES to the silica sol causes the collapse of the mesoporous silica pore structure, resulting in weaker peaks around $2\theta = 23°$. With the incorporation of MG nanosheets, a new characteristic peak is observed at $2\theta = 26°$, corresponding to the characteristic peak of graphite nanosheets [53,54], with the intensity of its diffraction peaks significantly increasing with content. A new weak characteristic peak corresponding to graphene is observed at $2\theta = 11°$, suggesting the conversion of certain graphite phases into graphene phases by exfoliation [55,56].

3.3. Adhesion test of composite coatings

The adhesion strength between the coating and substrate is a critical factor in assessing the stability of coatings. According to ISO 2409:2020, the adhesion between the coating and the substrate is measured by the cross-cut test. A square grid pattern is created on the surface of the coating by a cutting tool, with six cutting lanes in each direction of the grid. Subsequently, adhesive tape is applied to the surface and swiftly pulled off to assess adhesion. Fig. 7 illustrates obvious coating damage and shedding on the surface of the pure organosilicon coating sample (NBR-MG0), with severe shedding observed on both sides of the scratch and at the vertical cross position. The MG nanosheets improve the surface damage of NBR-MG2 and NBR-MG4, with only minimal coating spalling around the scratch and at the vertical intersection. With further increase in the MG content, almost no coating shedding is observed from the surface of NBR-MG6 and NBR-MG8, and all the scratches exhibit smooth cutting paths. These results demonstrate that MG effectively enhances the adhesion between the coating and the substrate. The modification of graphite nanosheets with KH-550 creates covalent bonds with the substrate, serving as a connecting bridge between the substrate and the organosilicon sol and enhancing the interface interaction, which is confirmed by FTIR (Fig. 3). The adhesion strengths of the coated sample are presented in Table 2.

3.4. Wear resistance of composite coatings

Fig. 8 illustrates the friction coefficient trend over time under dry friction conditions. With increasing MG content, the friction coefficient curve decreases and then increases, reaching the minimum of 6 mg/ml MG content. NBR-MG6 exhibits the lowest friction coefficient (0.11) and wear rate, with a 90.8 % reduction in the friction coefficient compared to pure NBR (1.2). The two-dimensional wear profiles and maximum wear depths of different samples are shown in Figs. 9 and 10, respectively. NBR-MG6 shows the smallest wear depth and profile, while pure NBR displays the largest. With increasing MG content, the maximum wear depth of the samples initially decreases and then increases. Fig. 11 presents the three-dimensional morphology of the worn surfaces of different coatings. The coatings on NBR-MG0 and NBR-MG2 are destroyed during the wear process, and the wear tracks penetrate deep into the substrate, which leads to a rapid increase in the friction coefficient of the two coating samples at the later stage of wear. Particles shed by the coating and abrasive debris falling off from the surface of the

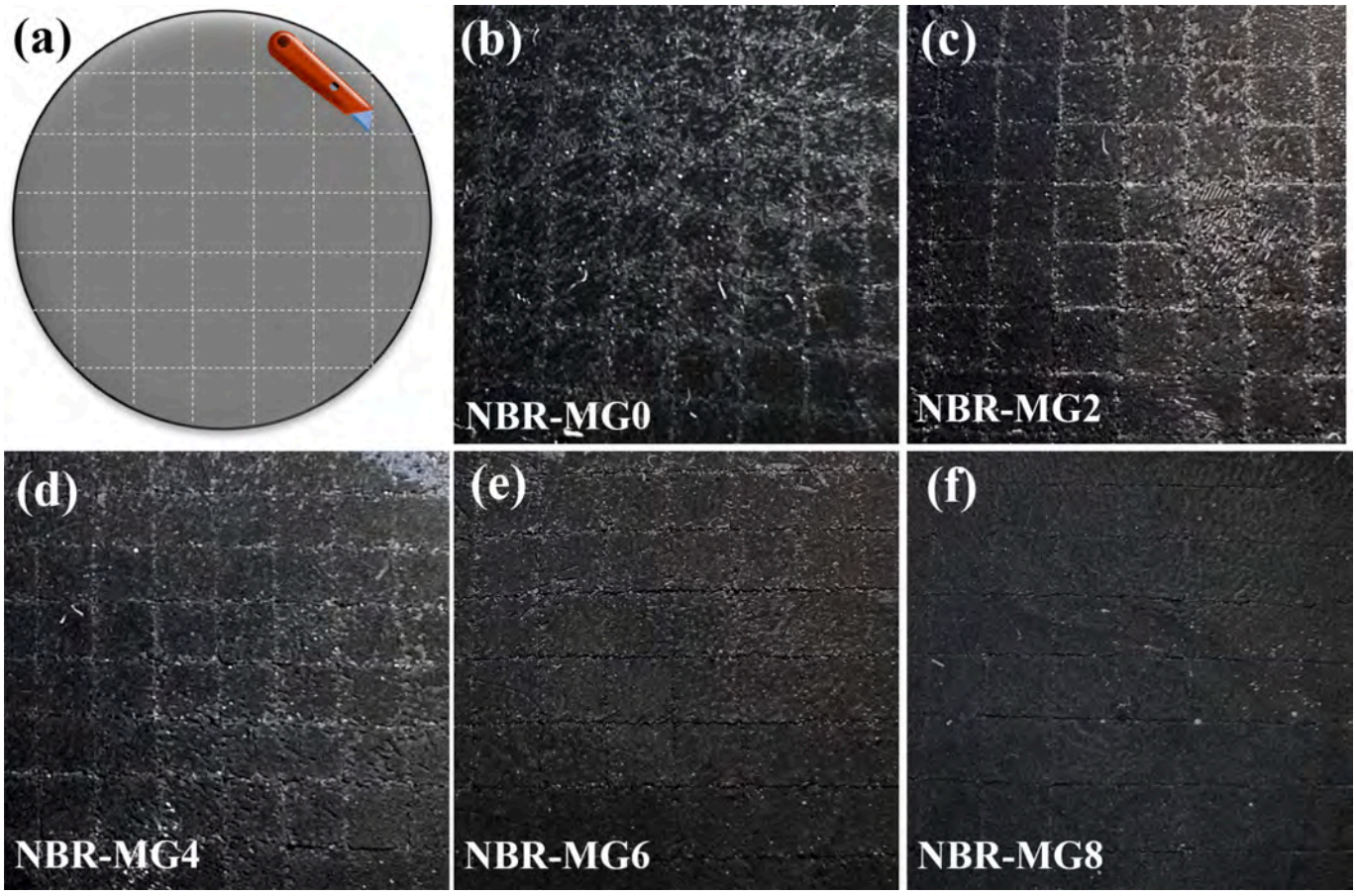

Fig. 7. (a) Schematic image of the cross-cut test; Digital pictures of the coatings after shedding: (b) NBR-MG0, (c) NBR-MG2, (d) NBR-MG4, (e) NBR-MG6, (f) NBR-MG8.

Table 2
Adhesion grade of the coated samples.

Samples	Adhesion grade
NBR-MG0	3 (15 % < shedding area < 35 %)
NBR-MG2	2 (5 % < shedding area < 15 %)
NBR-MG4	1 (0 < shedding area < 5 %)
NBR-MG6	0 (no shedding)
NBR-MG8	0 (no shedding)

ball cause three-body abrasive wear, which increases the friction coefficient and intensifies the wear of the materials. Moreover, NBR-MG8 exhibits extensive coating exfoliation in the wear areas, with some regions of the substrate surface exposed, which may be related to the holes and defects inside the coating (Fig. 5(j)). Fortunately, the coatings on NBR-MG4 and NBR-MG6 not only remain intact on the surface, but do not separate from the substrate. The above results show that too little or too much MG in the coatings can lead to deterioration in the friction and wear performance of the coatings.

According to the wear results of the coated samples, the wear resistance mechanism of the composite coatings is discussed (Fig. 12). In this study, MG nanosheets are incorporated into the organosilicon as the lubricant phase to form a "soft-hard" self-lubricating wear-resistant coating, where the organosilicon acts as a wear-resistant and supporting phase in the friction and wear process. The MG nanosheets serve as the source of the lubricant film on the friction surface, with their content being crucial for the continuous formation and replenishment of the film. It has been widely confirmed that silane coupling agent (e.g., KH-550) can improve the adhesion between the coating and the substrate by enhancing the interfacial interaction between the materials [57–59].

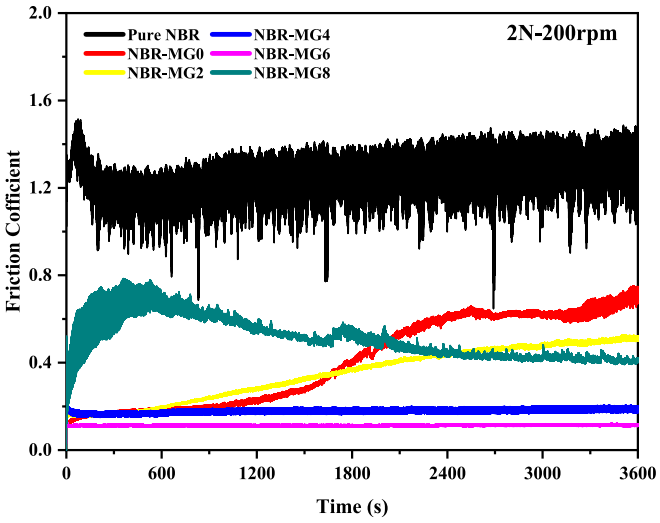

Fig. 8. Friction coefficients of different coated samples.

FTIR results indicate that the (SiOH) bonds generated by the hydrolysis of KH-550 successfully graft onto the surface of the graphite sheets, allowing these groups to bond with both the substrate and the organosilicon. Furthermore, adhesion tests reveal that compared to NBR-MG0, the adhesion of NBR-MG2 is significantly improved. Combined with the wear results, it is found that the coating of NBR-MG0 completely sheds off along the friction path, while the coating of NBR-MG2 shows partial

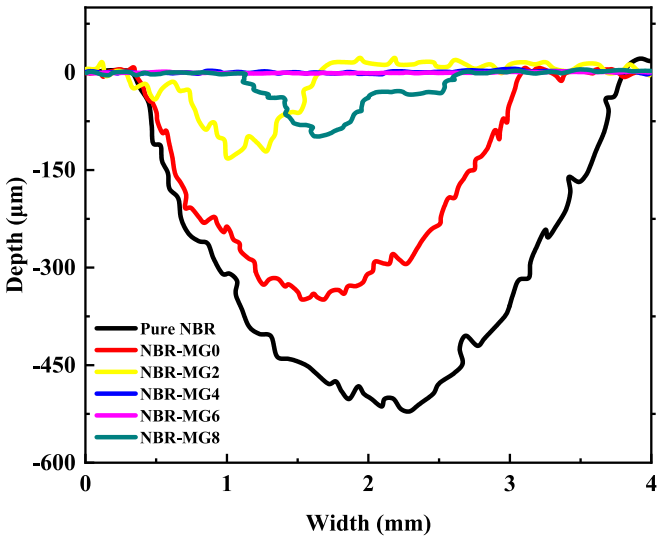

Fig. 9. 2D profiles of different coated samples.

shedding, but its overall wear resistance is significantly improved. This suggests that the introduction of MG enhances the bonding strength between the organosilicon coating and the substrate, thereby improving the wear resistance of coatings. Due to the relatively low adhesion of the NBR-MG0 and NBR-MG2 coatings, organosilicon detachment occurs during wear. The hard debris formed by the shedding of organosilicon collects on the wear surface and further aggravates the wear process (Fig. 12(a)). For NBR-MG4 and NBR-MG6, both the friction coefficient and wear rate are relatively low (with NBR-MG6 having the lowest values), and the coating remains intact after wear without any significant detachment. The application of graphite in lubrication has been extensively investigated in the literature, where it acts as a lubricating phase that forms a lubricating film during the wear process [40–42]. Therefore, the wear resistance of NBR-MG4 and NBR-MG6 may be attributed to the formation of a self-lubricating film by MG nanosheets during friction, and the appropriate amount of graphite can achieve the best lubrication effect, thus reducing the friction coefficient (Fig. 12(b)). The coatings of NBR-MG8 exhibit a small range of shedding phenomenon after wear, with the shedding area being relatively homogeneous. Fig. 5(j) shows that noticeable voids appear in the coating cross-section, indicating that excessive aggregation of MG nanosheets can lead to defects in the coating (Fig. 12(c)), making it more prone to wear failure [60,61]. Additionally, an excess of MG nanosheets hinder the coating from fully utilizing the self-lubricating properties of the MG nanosheets, although some lubrication is still provided.

3.5. Hydrogen barrier properties of composite coatings

According to ISO 15105-1, ASTM D1434–82, the hydrogen barrier properties are determined by the differential pressure method. The hydrogen permeability coefficients of the samples are calculated by monitoring the pressure change in the low-pressure chamber over time. The hydrogen diffusivity coefficient is determined using the time-lag method, while the hydrogen solubility is obtained by the ratio of the hydrogen permeability coefficient to the hydrogen diffusivity coefficient. Fig. 13(b) and (c) shows that pure NBR has the highest hydrogen permeability and diffusivity coefficient of 4.331×10^{-9} ($mol \cdot m^{-1} \cdot s^{-1} \cdot MPa^{-1}$) and 4.161×10^{-10} (m^2/s), respectively. For the sample with pure organosilicon, there is a slight decrease in the hydrogen permeability and diffusivity coefficient, indicating that the organosilicon plays a physical barrier role to a certain extent. As the MG content increases, there is a downward trend in both the hydrogen permeability and diffusivity coefficient of the sample, with a more pronounced decrease observed in the diffusivity coefficient. Upon increasing the doping quantity of MG to 8 mg/ml, the hydrogen permeability and diffusivity coefficient decrease to 2.031×10^{-9} ($mol \cdot m^{-1} \cdot s^{-1} \cdot MPa^{-1}$) and 1.862×10^{-10} (m^2/s), representing a reduction of 53 % and 81 %, respectively. In addition, the solubility coefficient slightly decreases when the sample surface is coated with a pure organosilicon, suggesting that the cross-linked molecules in the coating exhibit extremely weak adsorption capacity for hydrogen (Fig. 13(d)). However, with the increase of the content of MG in the coating, the hydrogen solubility of the sample gradually increases and is higher than that of the pure NBR sample (Fig. 13(d)). This suggests that the graphite sheet acts as both a barrier to hinder hydrogen diffusion and an adsorbent for diffused hydrogen molecules in its vicinity, thereby enhancing hydrogen solubility. The above results indicate that the hydrogen permeation behavior of the sample primarily relies on diffusion rather

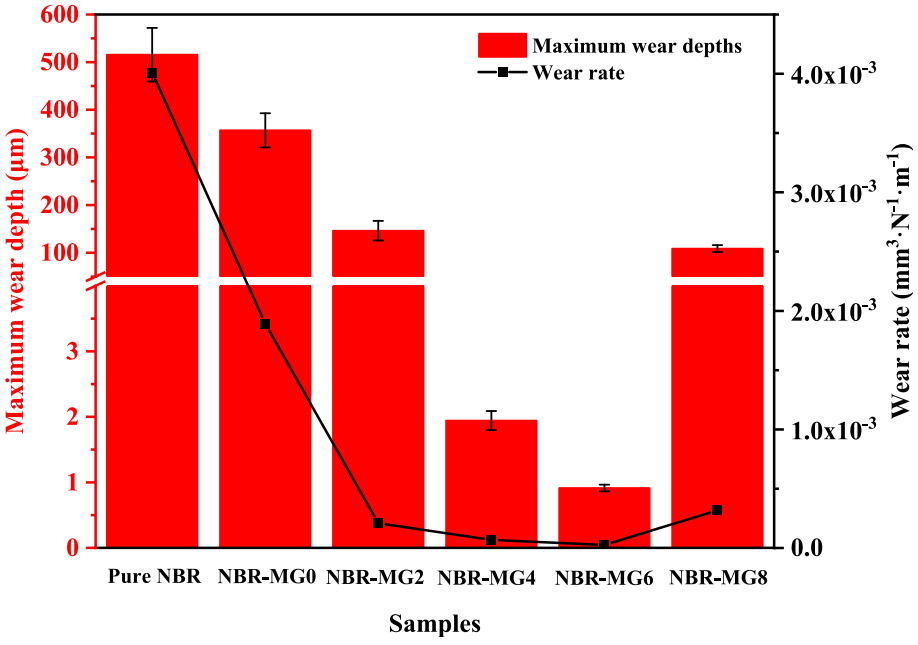

Fig. 10. Maximum wear depths and wear rates of different coated samples.

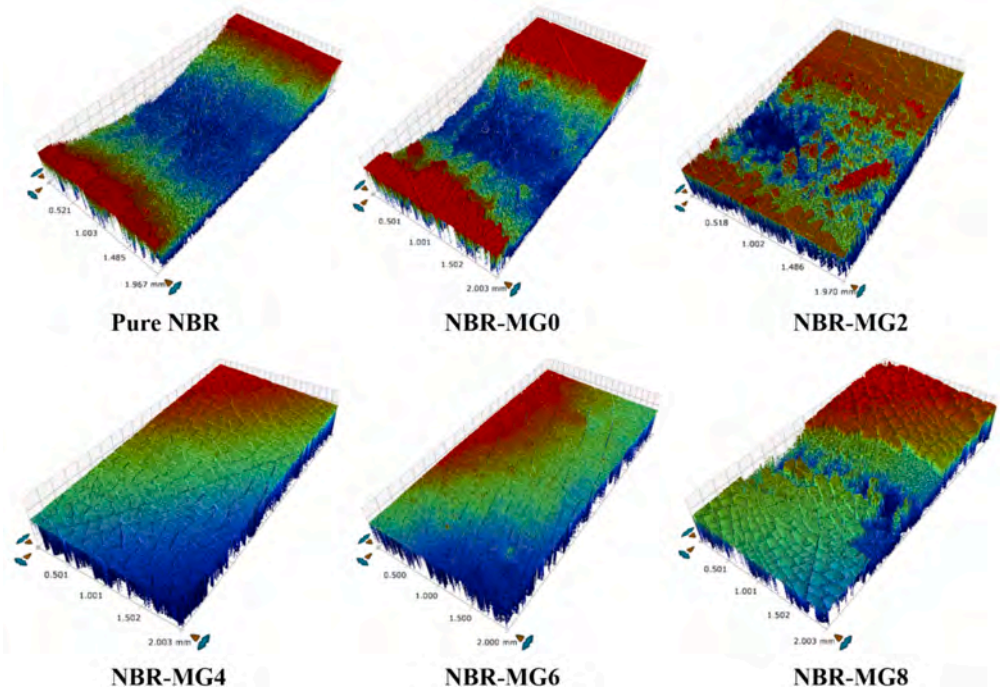

Fig. 11. 3D profile of the wear scars on different samples.

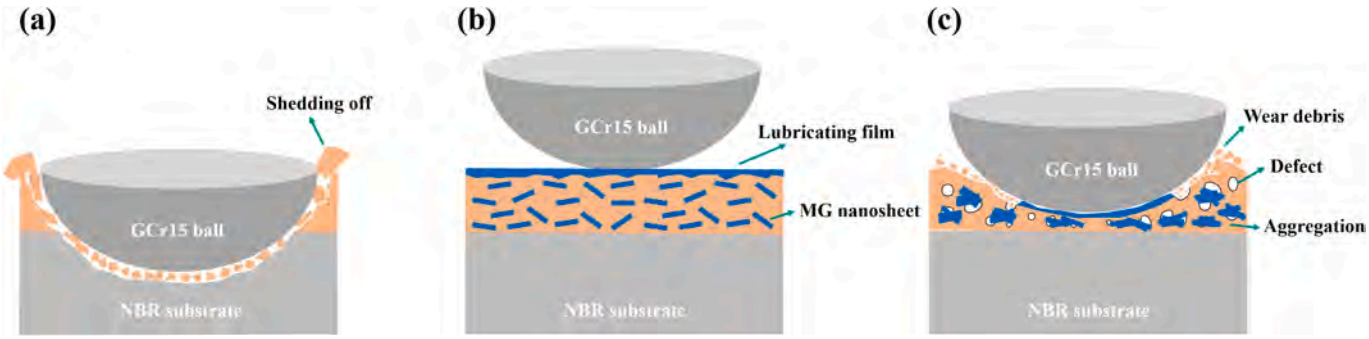

Fig. 12. Wear resistance mechanism of the composite coating: (a) the coating with no or small amount of MG nanosheets; (b) the coating with appropriate amount of MG nanosheets; (c) the coating with excessive MG nanosheets.

than dissolution. Hydrogen permeation parameters of different samples are presented in Table 3, and the hydrogen permeability coefficient is equal to the product of hydrogen diffusivity coefficient and hydrogen solubility coefficient.

The permeation reduction factor (*PRF*) is usually used as an indicator to quantify the degree of permeation reduction of the coating relative to the substrate. Under specific upstream pressure and temperature conditions, the steady state ratio of the permeation rate of the uncoated substrate $j_{uncoated}$ to the permeation rate of the coated substrate j_{coated} is called the *PRF* [62,63]:

$$PRF = \frac{j_{uncoated}}{j_{coated}} \tag{1}$$

For the coated substrate, hydrogen permeates through both layers of material. The relationship between uncoated and coated substrate and the hydrogen permeability coefficient is shown as follows:

$$j_{uncoated} = \frac{P_1}{d_1} \tag{2}$$

$$j_{coated} = \frac{P}{d_1 + d_2} = \left(\frac{d_1}{P_1} + \frac{d_2}{P_2}\right)^{-1} \tag{3}$$

where P is the total hydrogen permeability coefficient of the coated substrate, P_1 and P_2 are the hydrogen permeability coefficients of the substrate and coating, respectively, and d_1 and d_2 are the thicknesses of the substrate and coating, respectively. Combining Eq. (1), (2) and (3), *PRF* can be obtained:

$$PRF = 1 + \frac{d_2 P_1}{d_1 P_2} \tag{4}$$

According to the literature data, the *PRF* of hydrogen barrier coatings on polymer surfaces are calculated and compared with our work. According to the literature data, the *PRF* of hydrogen barrier coatings on polymer surfaces are calculated and compared with our work. As presented in Table 4, the range of *PRF* in the literature and this work are 1.73–57.58 and 1.17–2.15, respectively. Admittedly, the barrier properties of this study need to be further improved. However, it is undeniable that the composite coating with the functions of hydrogen barrier and wear resistance are innovatively constructed on the surface of the rubber in this study, showing great potential in the field of high-pressure hydrogen dynamic sealing.

Hydrogen molecules leak into the external environment through rubber seals or accumulate inside the materials to cause hydrogen-

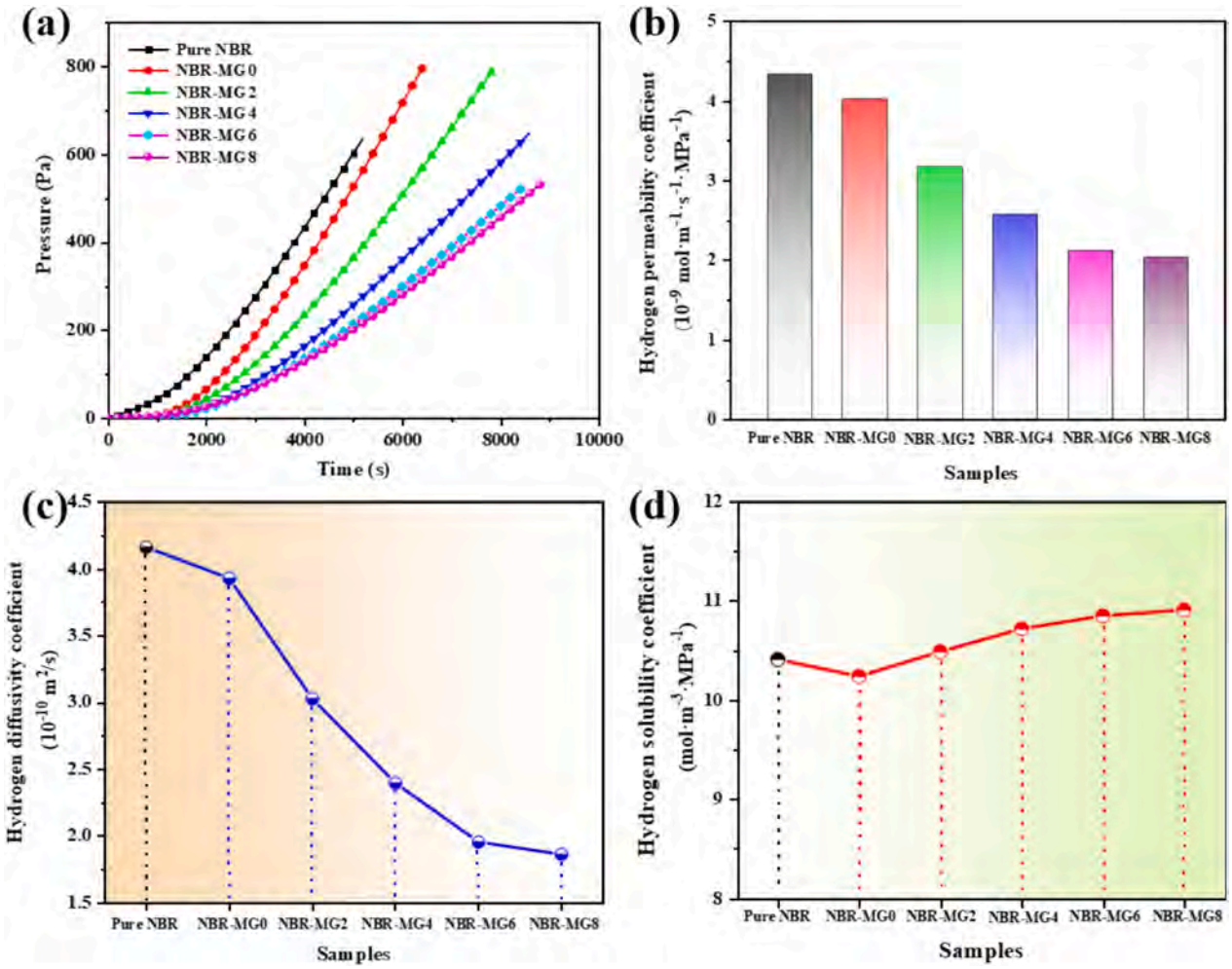

Fig. 13. (a) Curves of the pressure in the lower chamber of the instrument with increasing permeation time; (b) hydrogen permeability coefficient; (c) hydrogen diffusivity coefficient; (d) hydrogen solubility coefficient of different samples.

Table 3
Hydrogen permeation parameters of different samples.

Samples	Hydrogen permeability coefficient ($mol \cdot m^{-1} \cdot s^{-1} \cdot MPa^{-1}$)	Hydrogen diffusivity coefficient (m^2/s)	Hydrogen solubility coefficient ($mol \cdot m^{-3} \cdot MPa^{-1}$)
Pure NBR	4.331×10^{-9}	4.161×10^{-10}	10.41
NBR-MG0	4.022×10^{-9}	3.928×10^{-10}	10.24
NBR-MG2	3.175×10^{-9}	3.027×10^{-10}	10.49
NBR-MG4	2.568×10^{-9}	2.396×10^{-10}	10.72
NBR-MG6	2.120×10^{-9}	1.954×10^{-10}	10.85
NBR-MG8	2.031×10^{-9}	1.862×10^{-10}	10.91

induced damage, posing safety hazards to high-pressure hydrogen sealing. Reducing hydrogen permeation through coatings is a feasible solution. Prior to reaching the rubber substrate, hydrogen molecules must overcome internal barriers in the composite coating, as shown in Fig. 14. The layered MG nanosheets uniformly distributed in the organosilicon reduce the available volume for the free diffusion of hydrogen molecules. Moreover, the MG nanosheets have strong hydrogen molecule adsorption capacity, and hydrogen molecules diffusing into their vicinity will be captured. In fact, hydrogen adsorption can be categorized into two forms of chemical adsorption and physical adsorption [44–46,65]: (1) similar to graphene, unsaturated dangling bonds in graphite nanosheets combine with hydrogen atoms to form C—H sp^3 bonds and (2) graphite nanosheets serve as typical hydrogen storage materials, physically adsorbing hydrogen molecules between graphite layers. It is evident that with increasing content of MG nanosheets, their adsorption capacity for hydrogen molecules also increases, but there is a limit to the overall adsorption capacity, possibly due to the aggregation effects of graphite nanosheets. The results explain the changes in the hydrogen solubility of the coatings with different contents of MG during the permeation experiments, and the trends pertaining to the adsorption of hydrogen molecules by graphite nanosheets. When both adsorption modes reach saturation, hydrogen adsorption will no longer continue, and the remaining hydrogen molecules, unable to penetrate the dense graphite nanosheets, can only continue to diffuse downward along the edges of the graphite nanosheets. With increasing MG content, the uniformly arranged graphite nanosheets form multilayer physical barriers to extend the diffusion path of hydrogen molecules and reduce the hydrogen diffusivity coefficient. In conclusion, the hydrogen barrier properties of composite coatings are primarily attributed to the adsorption of hydrogen molecules by the MG nanosheets and the extension of the diffusion path [35,64,66].

Table 4
Hydrogen permeability coefficients and *PRF* for different coated samples.

Materials	P (mol·m^{-1}·s^{-1}·MPa^{-1})	P_1 (mol·m^{-1}·s^{-1}·MPa^{-1})	P_2 (mol·m^{-1}·s^{-1}·MPa^{-1})	*PRF*
Nylon coated samples [7]	0.27–1.85 × 10^{-10}	3.68 × 10^{-10}	0.113–1.63 × 10^{-12}	2.04–13.71
Nylon coated samples [28]	5.2–16.7 × 10^{-10}	28.8 × 10^{-10}	2.02–7.81 × 10^{-12}	1.73–5.63
PET coated samples [26]	0.046–0.28 × 10^{-10}	0.95 × 10^{-10}	0.145–3.05 × 10^{-12}	1.96–57.58
PET coated samples [27]	0.53–0.75 × 10^{-10}	0.916 × 10^{-10}	4.56–6.97 × 10^{-11}	4.15–6.22
PET coated samples [47]	1.58–2.06 × 10^{-10}	2.3 × 10^{-10}	1.13–1.83 × 10^{-10}	2.03–2.59
PET coated samples [64]	1.96–2.66 × 10^{-10}	2.8 × 10^{-10}	1.67–2.56 × 10^{-10}	2.36–3.93
NBR coated samples (this work)	2.031–4.022 × 10^{-9}	4.331 × 10^{-9}	0.342–3.89 × 10^{-10}	1.17–2.15

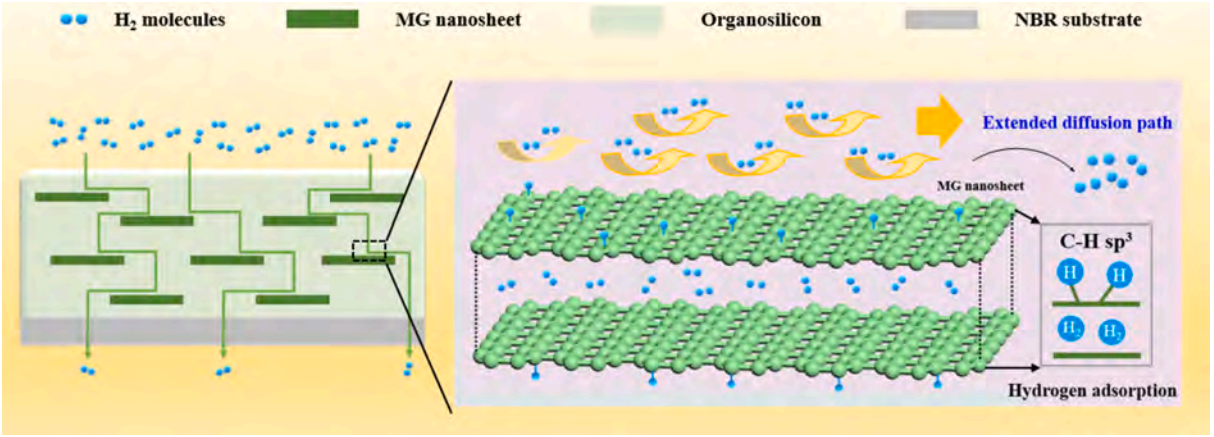

Fig. 14. Hydrogen barrier mechanism of the composite coating.

4. Conclusion

A "soft-hard combination" composite coating comprising MG nanosheets and organosilicon is designed and prepared on rubber surfaces to improve the wear resistance and lower the permeability of rubber seals in hydrogen equipment. The incorporation of MG nanosheets significantly enhances the wear resistance and hydrogen barrier properties of the composite coatings. Compared to the pure NBR substrate, NBR-MG6 exhibits a 90.8 % decrease in the friction coefficient and a 51 % decrease in the hydrogen permeability coefficient. The wear resistance mechanism of the composite coating may be attributed to the enhancement of the adhesion of the MG nanosheet to the coating and the formation of the self-lubricating film. Furthermore, MG nanosheets form a barrier layer within the coating, extending the diffusion path of hydrogen molecules and adsorbing nearby hydrogen, thereby reducing the permeability. This work reveals a feasible solution for anti-wear and friction reduction and hydrogen damage resistance control of rubber seals in hydrogen energy equipment.

CRediT authorship contribution statement

Chilou Zhou: Writing – review & editing, Supervision, Resources, Funding acquisition, Conceptualization. **Yanlei Huang:** Writing – original draft, Visualization, Methodology, Investigation, Formal analysis. **Xianhui Liu:** Writing – original draft, Investigation, Conceptualization. **Yan Huang:** Investigation, Data curation. **Hao Wu:** Writing – review & editing, Supervision, Project administration, Methodology. **Zhengli Hua:** Visualization, Methodology, Investigation. **Paul K. Chu:** Writing – review & editing, Supervision, Funding acquisition. **Yansheng Yin:** Writing – review & editing, Funding acquisition.

Declaration of competing interest

The authors declare that they have no known competing financial interests or personal relationships that could have appeared to influence the work reported in this paper.

Acknowledgments

This research is supported by the National Natural Science Foundation of China (No. 52075183 and No. 52371059), Guangdong Basic and Applied Basic Research Foundation (No. 2023A1515010692), Open Project of Technology Innovation Center of Hydrogen Storage-Transportation and Fueling Equipments, State Administration for Market Regulation (No. TICHE2024002), Guangdong Provincial Administration for Market Regulation Funds of Science and Technology (No. 2022ZT01), City University of Hong Kong Strategic Research Grant (SRG 7005505), and City University of Hong Kong Donation Research Grants (DON-RMG 9229021 and 9220061).

Data availability

Data will be made available on request.

References

[1] S. Bosu, N. Rajamohan, Recent advancements in hydrogen storage - comparative review on methods, operating conditions and challenges, Int. J. Hydrog. Energy 52 (2024) 352–370, https://doi.org/10.1016/j.ijhydene.2023.01.344.
[2] B.S. Zainal, P.J. Ker, H. Mohamed, H.C. Ong, I.M.R. Fattah, S.M.A. Rahman, L. D. Nghiem, T.M.I. Mahlia, Recent advancement and assessment of green hydrogen production technologies, Renew. Sust. Energ. Rev. 189 (2024) 113941, https://doi.org/10.1016/j.rser.2023.113941.
[3] C. Zhou, P. Dai, H. Wu, M. Xia, J. Xue, Y. Huang, P.K. Chu, Optimizing hydrogen permeation properties of WS2-Ni composite coatings on pipeline steel for improved hydrogen protection, Surf. Coat. Technol. 488 (2024) 131053, https://doi.org/10.1016/j.surfcoat.2024.131053.
[4] D. Guan, B. Wang, J. Zhang, R. Shi, K. Jiao, L. Li, Y. Wang, B. Xie, Q. Zhang, J. Yu, Y. Zhu, Z. Shao, M. Ni, Hydrogen society: from present to future, Energy Environ. Sci. 16 (11) (2023) 4926–4943, https://doi.org/10.1039/d3ee02695g.
[5] P. Halder, M. Babaie, F. Salek, N. Haque, R. Savage, S. Stevanovic, T.A. Bodisco, A. Zare, Advancements in hydrogen production, storage, distribution and refuelling for a sustainable transport sector: hydrogen fuel cell vehicles, Int. J. Hydrog. Energy (2023) 973–1004, https://doi.org/10.1016/j.ijhydene.2023.07.204.

[6] H. Fujiwara, H. Ono, K. Onoue, S. Nishimura, High-pressure gaseous hydrogen permeation test method-property of polymeric materials for high-pressure hydrogen devices (1), Int. J. Hydrog. Energy 45 (53) (2020) 29082–29094, https://doi.org/10.1016/j.ijhydene.2020.07.215.
[7] O.B. Seo, S. Saha, N.H. Kim, J.H. Lee, Preparation of functionalized MXene-stitched-graphene oxide/poly (ethylene-co-acrylic acid) nanocomposite with enhanced hydrogen gas barrier properties, J. Membr. Sci. 640 (2021) 119839, https://doi.org/10.1016/j.memsci.2021.119839.
[8] P. Li, K. Chen, L. Zhao, H. Zhang, H. Sun, X. Yang, N.H. Kim, J.H. Lee, Q.J. Niu, Preparation of modified graphene oxide/polyethyleneimine film with enhanced hydrogen barrier properties by reactive layer-by-layer self-assembly, Compos. Part B-Eng. 166 (2019) 663–672, https://doi.org/10.1016/j.compositesb.2019.02.058.
[9] S.K. Jeon, J.K. Jung, N.K. Chung, U.B. Baek, S.H. Nahm, Investigation of physical and mechanical characteristics of rubber materials exposed to high-pressure hydrogen, Polymers 14 (11) (2022) 2233, https://doi.org/10.3390/polym14112233.
[10] B. Sebők, M. Schülke, F. Réti, G. Kiss, Diffusivity, permeability and solubility of H2, Ar, N2, and CO2 in poly(tetrafluoroethylene) between room temperature and 180 °C, Polym. Test. 49 (2016) 66–72, https://doi.org/10.1016/j.polymertesting.2015.10.016.
[11] W. Balasooriya, C. Clute, B. Schrittesser, G. Pinter, A review on applicability, limitations, and improvements of polymeric materials in high-pressure hydrogen gas atmospheres, Polym. Rev. 62 (1) (2021) 175–209, https://doi.org/10.1080/15583724.2021.1897997.
[12] C. Zhou, Y. Zheng, Z. Hua, W. Mou, X. Liu, Recent insights into hydrogen-induced blister fracture of rubber sealing materials: an in-depth examination, Polym. Degrad. Stab. 224 (2024) 110747, https://doi.org/10.1016/j.polymdegradstab.2024.110747.
[13] J. Yamabe, S. Nishimura, Influence of fillers on hydrogen penetration properties and blister fracture of rubber composites for O-ring exposed to high-pressure hydrogen gas, Int. J. Hydrog. Energy 34 (4) (2009) 1977–1989, https://doi.org/10.1016/j.ijhydene.2008.11.105.
[14] C. Zhou, X. Liu, Y. Zheng, Z. Hua, A comprehensive review of hydrogen-induced swelling in rubber composites, Compos. Part B-Eng. 275 (2024) 111342, https://doi.org/10.1016/j.compositesb.2024.111342.
[15] H. Fujiwara, H. Ono, S. Nishimura, Effects of fillers on the hydrogen uptake and volume expansion of acrylonitrile butadiene rubber composites exposed to high pressure hydrogen: property of polymeric materials for high pressure hydrogen devices (3), Int. J. Hydrog. Energy 47 (7) (2022) 4725–4740, https://doi.org/10.1016/j.ijhydene.2021.11.061.
[16] B.L. Choi, J.K. Jung, U.B. Baek, B.H. Choi, Effect of functional fillers on tribological characteristics of acrylonitrile butadiene rubber after high-pressure hydrogen exposures, Polymers 14 (5) (2022) 861, https://doi.org/10.3390/polym14050861.
[17] E.R. Duranty, T.J. Roosendaal, S.G. Pitman, J.C. Tucker, S.L. Owsley Jr., J.D. Suter, K.J. Alvine, An in situ tribometer for measuring friction and wear of polymers in a high pressure hydrogen environment, Rev. Sci. Instrum. 88 (9) (2017) 095114, https://doi.org/10.1063/1.5001836.
[18] A. Milionis, J. Languasco, E. Loth, I.S. Bayer, Analysis of wear abrasion resistance of superhydrophobic acrylonitrile butadiene styrene rubber (ABS) nanocomposites, Chem. Eng. J. 281 (2015) 730–738, https://doi.org/10.1016/j.cej.2015.06.086.
[19] A. Sidorenko, H.-S. Ahn, D.-I. Kim, H. Yang, V. Tsukruk, Wear stability of polymer nanocomposite coatings with trilayer architecture, Wear 252 (11–12) (2002) 946–955, https://doi.org/10.1016/S0043-1648(02)00048-0.
[20] Y. Xu, J. Jia, G. Zhang, H. Li, T. Chen, Effect of rubber substrates on the flexibility and tribological properties of diamond-like carbon coatings, Surf. Coat. Technol. 422 (2021) 127526, https://doi.org/10.1016/j.surfcoat.2021.127526.
[21] X. Xu, Q. Li, F. Su, J. Sun, W. Li, In-situ formation of onion-like carbon film by tribo-induced catalytic degradation of hydrocarbon: effect of lubrication condition and load, Chem. Eng. J. 459 (2023) 141566, https://doi.org/10.1016/j.cej.2023.141566.
[22] T. Nakahigashi, Y. Tanaka, K. Miyake, H. Oohara, Properties of flexible DLC film deposited by amplitude-modulated RF P-CVD, Tribol. Int. 37 (11–12) (2004) 907–912, https://doi.org/10.1016/j.triboint.2004.07.007.
[23] B. Zhou, Z. Liu, B. Xu, A. Rogachev, M. Yarmolenko, A. Rogachev, Modification of Cu-PE-PTFE composite coatings on rubber surface by low-energy electron beam dispersion with glow discharge, Polym. Eng. Sci. 58 (1) (2018) 103–111, https://doi.org/10.1002/pen.24536.
[24] M. Bragaglia, I. Cacciotti, V. Cherubini, F. Nanni, Influence of organic modified silica coatings on the tribological properties of elastomeric compounds, Wear 434 (2019) 202987, https://doi.org/10.1016/j.wear.2019.202987.
[25] P. Bandyopadhyay, T.T. Nguyen, X. Li, N.H. Kim, J.H. Lee, Enhanced hydrogen gas barrier performance of diaminoalkane functionalized stitched graphene oxide/polyurethane composites, Compos. Part B-Eng. 117 (2017) 101–110, https://doi.org/10.1016/j.compositesb.2017.02.035.
[26] W.B. Park, P. Bandyopadhyay, T.T. Nguyen, T. Kuila, N.H. Kim, J.H. Lee, Effect of high molecular weight polyethyleneimine functionalized graphene oxide coated polyethylene terephthalate film on the hydrogen gas barrier properties, Compos. Part B-Eng. 106 (2016) 316–323, https://doi.org/10.1016/j.compositesb.2016.09.048.
[27] S. Yuan, Y. Sun, C. Yang, Y. Zhang, C. Cong, Y. Yuan, D. Lin, L. Pei, Y. Zhu, H. Wang, A novel dual-functional epoxy-based composite coating with exceptional anti-corrosion and enhanced hydrogen gas barrier properties, Chem. Eng. J. 449 (2022) 137876, https://doi.org/10.1016/j.cej.2022.137876.
[28] P. Bandyopadhyay, W.B. Park, R.K. Layek, M.E. Uddin, N.H. Kim, H.-G. Kim, J. H. Lee, Hexylamine functionalized reduced graphene oxide/polyurethane nanocomposite-coated nylon for enhanced hydrogen gas barrier film, J. Membr. Sci. 500 (2016) 106–114, https://doi.org/10.1016/j.memsci.2015.11.029.
[29] L. Zhao, H. Sun, N. Kim, J. Lee, Y. Kong, P. Li, Hydrogen gas barrier property of polyelectrolyte/GO layer-by-layer films, J. Appl. Polym. Sci. 132 (20) (2015), https://doi.org/10.1002/app.41973.
[30] L. Zhao, B. Yuan, Y. Geng, C. Yu, N.H. Kim, J.H. Lee, P. Li, Fabrication of ultrahigh hydrogen barrier polyethyleneimine/graphene oxide films by LBL assembly fine-tuned with electric field application, Compos. Part A-Appl. S. 78 (2015) 60–69, https://doi.org/10.1016/j.compositesa.2015.07.020.
[31] L. Zhao, H. Zhang, N.H. Kim, D. Hui, J.H. Lee, Q. Li, H. Sun, P. Li, Preparation of graphene oxide/polyethyleneimine layer-by-layer assembled film for enhanced hydrogen barrier property, Compos. Part B-Eng. 92 (2016) 252–258, https://doi.org/10.1016/j.compositesb.2016.02.037.
[32] R.M. Cadambi, E. Ghassemieh, Hard coatings on elastomers for reduced permeability and increased wear resistance, Plast. Rubber Compos. 41 (4–5) (2013) 169–174, https://doi.org/10.1179/1743289811y.0000000048.
[33] S. Saha, W. Son, N.H. Kim, J.H. Lee, Fabrication of impermeable dense architecture containing covalently stitched graphene oxide/boron nitride hybrid nanofiller reinforced semi-interpenetrating network for hydrogen gas barrier applications, J. Mater. Chem. A 10 (8) (2022) 4376–4391, https://doi.org/10.1039/d1ta09486f.
[34] X. Li, M. Guo, P. Bandyopadhyay, Q. Lan, H. Xie, G. Liu, X. Liu, X. Cheng, N.H. Kim, J.H. Lee, Two-dimensional materials modified layered double hydroxides: a series of fillers for improving gas barrier and permselectivity of poly(vinyl alcohol), Compos. Part B-Eng. 207 (2021) 108568, https://doi.org/10.1016/j.compositesb.2020.108568.
[35] K. Shi, S. Xiao, Q. Ruan, H. Wu, G. Chen, C. Zhou, S. Jiang, K. Xi, M. He, P.K. Chu, Hydrogen permeation behavior and mechanism of multi-layered graphene coatings and mitigation of hydrogen embrittlement of pipe steel, Appl. Surf. Sci. 573 (2022) 151529, https://doi.org/10.1016/j.apsusc.2021.151529.
[36] A. Al-Jabareen, H. Al-Bustami, H. Harel, G. Marom, Improving the oxygen barrier properties of polyethylene terephthalate by graphite nanoplatelets, J. Appl. Polym. Sci. 128 (3) (2012) 1534–1539, https://doi.org/10.1002/app.38302.
[37] K. Bilisik, M. Akter, Polymer nanocomposites based on graphite nanoplatelets (GNPs): a review on thermal-electrical conductivity, mechanical and barrier properties, J. Mater. Sci. 57 (15) (2022) 7425–7480, https://doi.org/10.1007/s10853-022-07092-0.
[38] W. Jiao, M. Shioya, R. Wang, F. Yang, L. Hao, Y. Niu, W. Liu, L. Zheng, F. Yuan, L. Wan, X. He, Improving the gas barrier properties of Fe3O4/graphite nanoplatelet reinforced nanocomposites by a low magnetic field induced alignment, Compos. Sci. Technol. 99 (2014) 124–130, https://doi.org/10.1016/j.compscitech.2014.05.022.
[39] A. Malas, C.K. Das, Influence of modified graphite flakes on the physical, thermo-mechanical and barrier properties of butyl rubber, J. Alloys Compd. 699 (2017) 38–46, https://doi.org/10.1016/j.jallcom.2016.12.232.
[40] V.M. Candelario, O. Borrero-López, F. Guiberteau, R. Moreno, A.L. Ortiz, Sliding-wear resistance of liquid-phase-sintered SiC containing graphite nanodispersoids, J. Eur. Ceram. Soc. 34 (10) (2014) 2597–2602, https://doi.org/10.1016/j.jeurceramsoc.2014.02.033.
[41] M. Khadem, V.E. Pukha, O.V. Penkov, I.I. Khodos, A.A. Belmesov, G.V. Nechaev, E. N. Kabachkov, P.A. Karaseov, D.-E. Kim, Formation of wear-resistant graphite/diamond-like carbon nanocomposite coatings on Ti using accelerated C60-ions, Surf. Coat. Technol. 424 (2021) 127670, https://doi.org/10.1016/j.surfcoat.2021.127670.
[42] H. Tan, Y. Guo, D. Wang, Y. Cui, The development of a Cu@Graphite solid lubricant with excellent anti-friction and wear resistant performances in dry condition, Wear 488-489 (2022) 204181, https://doi.org/10.1016/j.wear.2021.204181.
[43] J.J. Tang, K. Liu, Q.Z. Yang, Y.H. Wang, P. Zhang, Y. Wang, L. Zhao, Q.Q. Fu, Z. H. Han, Y. Bai, The influence of size and distribution of graphite on the friction and wear behavior of Ni–graphite coatings, Surf. Coat. Technol. 252 (2014) 48–55, https://doi.org/10.1016/j.surfcoat.2014.04.063.
[44] E. Areou, G. Cartry, J.M. Layet, T. Angot, Hydrogen-graphite interaction: experimental evidences of an adsorption barrier, J. Chem. Phys. 134 (1) (2011) 014701, https://doi.org/10.1063/1.3518981.
[45] J. Petucci, C. LeBlond, M. Karimi, G. Vidali, Diffusion, adsorption, and desorption of molecular hydrogen on graphene and in graphite, J. Chem. Phys. 139 (4) (2013) 044706, https://doi.org/10.1063/1.4813919.
[46] Q. Wang, J.K. Johnson, Hydrogen adsorption on graphite and in carbon slit pores from path integral simulations, Mol. Phys. 95 (2) (2009) 299–309, https://doi.org/10.1080/00268979809483162.
[47] S. Yuan, K. Li, Y. Sun, C. Cong, Y. Liu, D. Lin, L. Pei, Y. Zhu, H. Wang, Designing functionalized graphene-stitched-SiC/fluoropolymer novel composite coating with excellent corrosion resistance and hydrogen diffusion barrier properties, Chem. Eng. J. 472 (2023) 144881, https://doi.org/10.1016/j.cej.2023.144881.
[48] S. Cai, Y. Zhang, H. Zhang, H. Yan, H. Lv, B. Jiang, Sol-gel preparation of hydrophobic silica antireflective coatings with low refractive index by base/acid two-step catalysis, ACS Appl. Mater. Interfaces 6 (14) (2014) 11470–11475, https://doi.org/10.1021/am501972y.
[49] Z. Wang, R. Qi, J. Wang, S. Qi, Thermal conductivity improvement of epoxy composite filled with expanded graphite, Ceram. Int. 41 (10) (2015) 13541–13546, https://doi.org/10.1016/j.ceramint.2015.07.148.
[50] Y. He, W. Li, G. Yang, H. Liu, J. Lu, T. Zheng, X. Li, A novel method for fabricating wearable, piezoresistive, and pressure sensors based on modified-graphite/polyurethane composite films, Materials 10 (7) (2017), https://doi.org/10.3390/ma10070684.

[51] P. Deshmukh, J. Bhatt, D. Peshwe, S. Pathak, Determination of silica activity index and XRD, SEM and EDS studies of amorphous SiO2 extracted from rice husk ash, T. Indian I. Metals 65 (1) (2011) 63–70, https://doi.org/10.1007/s12666-011-0071-z.
[52] Musyarofah, S. Soontaranon, W. Limphirat, Triwikantoro, S. Pratapa, XRD, WAXS, FTIR, and XANES studies of silica-zirconia systems, Ceram. Int. 45(12) (2019) 15660–15670. doi:https://doi.org/10.1016/j.ceramint.2019.05.078.
[53] Z.Q. Li, C.J. Lu, Z.P. Xia, Y. Zhou, Z. Luo, X-ray diffraction patterns of graphite and turbostratic carbon, Carbon 45 (8) (2007) 1686–1695, https://doi.org/10.1016/j.carbon.2007.03.038.
[54] W. Cai, X. Feng, B. Wang, W. Hu, B. Yuan, N. Hong, Y. Hu, A novel strategy to simultaneously electrochemically prepare and functionalize graphene with a multifunctional flame retardant, Chem. Eng. J. 316 (2017) 514–524, https://doi.org/10.1016/j.cej.2017.01.017.
[55] B. Yuan, C. Bao, L. Song, N. Hong, K.M. Liew, Y. Hu, Preparation of functionalized graphene oxide/polypropylene nanocomposite with significantly improved thermal stability and studies on the crystallization behavior and mechanical properties, Chem. Eng. J. 237 (2014) 411–420, https://doi.org/10.1016/j.cej.2013.10.030.
[56] B. Yuan, Y. Hu, X. Chen, Y. Shi, Y. Niu, Y. Zhang, S. He, H. Dai, Dual modification of graphene by polymeric flame retardant and $Ni(OH)_2$ nanosheets for improving flame retardancy of polypropylene, Compos. Part A-Appl. S. 100 (2017) 106–117, https://doi.org/10.1016/j.compositesa.2017.04.012.
[57] J. Gu, T. Bai, J. Dang, J. Feng, Q. Zhang, Surface functionalization of HMPBO fibers with MSA/KH550/GlycidylEthyl POSS and improved interfacial adhesion, Polym. Compos. 35 (3) (2013) 611–616, https://doi.org/10.1002/pc.22702.
[58] W. Zhang, J. Wang, H. Liu, Z. Zhang, J. Wang, L. Zhang, H. Wang, F. Wang, F. Duan, J. Liu, M. Li, C. Hang, H. Chen, Surface treatment of micron silver flakes with coupling agents for high-performance electrically conductive adhesives, Int. J. Adhes. Adhes. 122 (2023), https://doi.org/10.1016/j.ijadhadh.2022.103300.
[59] Q. Zheng, J. Lv, J. Zhang, J. Feng, Fabrication and application of icephobic silicone coatings on epoxy substrate, Prog. Org. Coat. 161 (2021) 106483, https://doi.org/10.1016/j.porgcoat.2021.106483.
[60] X. Fan, Y. Xia, S. Wu, D. Zhang, S. Oliver, X. Chen, L. Lei, S. Shi, Covalently immobilization of modified graphene oxide with waterborne hydroxyl acrylic resin for anticorrosive reinforcement of its coatings, Prog. Org. Coat. 163 (2022) 106685, https://doi.org/10.1016/j.porgcoat.2021.106685.
[61] J. Li, S. Wang, S. Zhu, A. Fu, R. Cai, N. Lv, Z. Yang, C. Wang, Y. Li, Effect of KH-550 modified reduced graphene oxide (MrGO) content on the corrosion resistance behavior of MrGO/Epoxy coatings in CO2-Cl- environment, Int. J. Electrochem. Sc. 17 (6) (2022) 22069, https://doi.org/10.20964/2022.06.07.
[62] N.-E. Laadel, M. El Mansori, N. Kang, S. Marlin, Y. Boussant-Roux, Permeation barriers for hydrogen embrittlement prevention in metals – a review on mechanisms, materials suitability and efficiency, Int. J. Hydrog. Energy 47 (76) (2022) 32707–32731, https://doi.org/10.1016/j.ijhydene.2022.07.164.
[63] V. Nemanič, Hydrogen permeation barriers: basic requirements, materials selection, deposition methods, and quality evaluation, Nucl. Mater. Energy 19 (2019) 451–457, https://doi.org/10.1016/j.nme.2019.04.001.
[64] S. Yuan, Y. Sun, C. Cong, Y. Liu, D. Lin, L. Pei, Y. Zhu, H. Wang, A bi-layer orientated and functionalized graphene-based composite coating with unique hydrogen gas barrier and long-term anti-corrosion performance, Carbon 205 (2023) 54–68, https://doi.org/10.1016/j.carbon.2023.01.027.
[65] Q. Wang, J.K. Johnson, Computer simulations of hydrogen adsorption on graphite nanofibers, J. Phys. Chem. B 103 (2) (1999) 277–281, https://doi.org/10.1021/jp9839100.
[66] A. Granja-DelRío, M. Alducin, J.I. Juaristi, M.J. López, J.A. Alonso, Absence of spillover of hydrogen adsorbed on small palladium clusters anchored to graphene vacancies, Appl. Surf. Sci. 559 (2021) 149835, https://doi.org/10.1016/j.apsusc.2021.149835.